Is the Swedish wastewater sector ready for a transition to source separation?

Citation for the original published paper (version of record):
Mc Conville, J., Kvarnström, E., Jonsson, H. et al (2017). Is the Swedish wastewater sector ready for a transition to source separation?. Desalination and Water Treatment, 91: 320-328.
http://dx.doi.org/10.5004/dwt.2017.20881

(article starts on next page)

Science of the Total Environment 949 (2024) 174810

Contents lists available at ScienceDirect

Science of the Total Environment

journal homepage: www.elsevier.com/locate/scitotenv

Vegetation increases global climate vulnerability risk by shifting climate zones in response to rising atmospheric CO_2

Mingzhu He [a,b], Jiangpeng Cui [c,*], Yonghong Yi [d,*], Hans W. Chen [e], Qian Zhang [f], Lili Li [g], Ling Huang [h], Songbai Hong [i]

[a] Joint International Research Laboratory of Catastrophe Simulation and Systemic Risk Governance, Beijing Normal University, Zhuhai 519087, China
[b] School of National Safety and Emergency Management, Beijing Normal University, Zhuhai 519807, China
[c] State Key Laboratory of Tibetan Plateau Earth System and Resources Environment (TPESRE), Institute of Tibetan Plateau Research, Chinese Academy of Sciences, Beijing 100101, China
[d] College of Surveying and Geo-Informatics, Tongji University, Shanghai 200092, China
[e] Department of Space, Earth and Environment, Chalmers University of Technology, SE-412 96 Gothenburg, Sweden
[f] School of Geomatics Science and Technology, Nanjing Tech University, Nanjing 211816, China
[g] West Yunnan University of Applied Sciences, Yunnan 671000, China
[h] Sino-French Institute for Earth System Science, College of Urban and Environmental Sciences, Peking University, Beijing 100871, China
[i] School of Urban Planning and Design, Shenzhen Graduate School, Peking University, Shenzhen 518055, China

HIGHLIGHTS

- 4 × CO_2 induces climate zone shifts over 51.2% of the global land area.
- Vegetation physiological responses to 4 × CO_2 contribute 16.8% of climate shifts.
- Vegetation-enhanced temperature dominates the corresponding climate shifts.
- Vegetation-driven precipitation change is also important to shift climate zones.

GRAPHICAL ABSTRACT

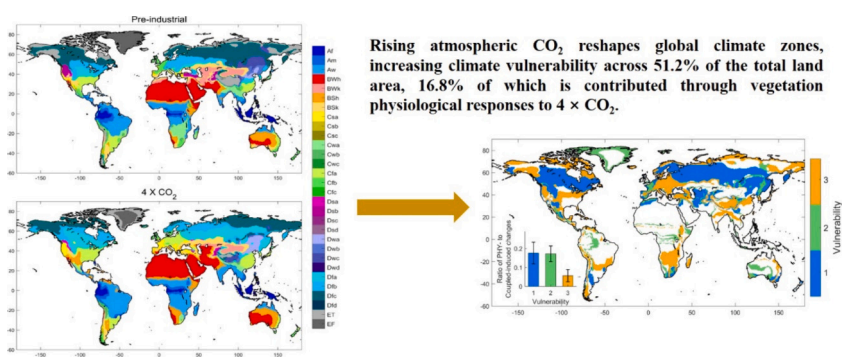

ARTICLE INFO

Editor: Yuyu Zhou

Keywords:
Climate zone shifts
Rising atmospheric CO_2
Vegetation physiological response
Climate vulnerability

ABSTRACT

Global climate zones are experiencing widespread shifts with ongoing rise in atmospheric CO_2, influencing vegetation growth and shifting its distributions to challenge ecosystem structure and function, posing threats on ecological and societal safety. However, how rising atmospheric CO_2 affects the pace of global climate zone shifts is highly uncertain. More attentions are urgently required to understand the underlying mechanisms and quantifications of regional climate vulnerability in response to rising CO_2. In this study, we employ nine Earth system models from CMIP6 to investigate global climate zone shifts with rising CO_2, unravel the effects of vegetation physiological response (PHY), and categorize climate vulnerable regions depending on the extent of climate zone shifts. We find that climate zone shifts over half of the global land area, 16.8% of which is contributed by PHY at 4 × CO_2. Intriguingly, besides warming, PHY-induced precipitation changes and their

* Corresponding authors.
E-mail addresses: cuijp@itpcas.ac.cn (J. Cui), yonghong_yi@tongji.edu.cn (Y. Yi).

https://doi.org/10.1016/j.scitotenv.2024.174810
Received 17 February 2024; Received in revised form 15 May 2024; Accepted 13 July 2024
Available online 23 July 2024

interactions with warming dominate about two-fifths of PHY-forced shifts, providing potential direction for model improvement in future predictions of climate zone shifts. Aided with PHY effects, 4 × CO_2 imposes substantial climate zone shifts over about one-fifth of the global land area, suggesting substantial changes in local climate and ecosystem structure and functions. Hence, those regions would experience strong climate vulnerability, and face high risk of climate extremes, water scarcity and food production. Our results quantitatively identify the vulnerable regions and unravel the underlying drivers, providing scientific insights to prioritize conservation and restoration efforts to ensure ecological and social safety globally.

1. Introduction

The increasing atmospheric CO_2 reshapes global climate zone distributions, imposing profound impacts on terrestrial ecosystems and human society. For example, expansions of warmer climate zones can lead to many species migrating to higher latitudes, resulting in changes of vegetation distributions and biodiversity, and influencing local ecosystem structures and function to threaten ecological safety (Chen et al., 2011; Rohli et al., 2015b, 2015a; Sohoulande, 2023). Spatial changes in soil organic carbon were align with climate zone transitions in Australian grasslands, pointing out their impacts on terrestrial carbon dynamics (Gibson et al., 2021). Importantly, steep-slope agricultural areas, which are important for food production, were much more affected by climate zone shifts than average global agricultural lands, especially by the expansion of arid zones (Wang et al., 2022). In addition, climate zone transitions accompanied with substantial precipitation changes could pose threats to irrigation supply and water scarcity, influencing food production (McDermid et al., 2023). Furthermore, ecosystem service values of 467–632 billion dollars (37%–50% of total ecosystem service value) are found in climate zone transitions by 2085 under RCP8.5 scenario, figuring out the critical impacts of climate zone changes on ecosystem service and economics (Watson et al., 2020). There is also a risk of future climate zone changes on population distributions (Skalák et al., 2018). Climate model projections using the RCP8.5 scenario predict that climate zone changes by the end of this century would affect 1.3–1.6 billion people (14–21% of the global population), especially in temperate regions under historical climate (Malone, 2023). Therefore, it is essential to reliably predict future climate zone shifts and unravel the underlying mechanisms to provide theoretical basis for climate mitigation. Comprehensive analyses are urgently needed to quantitatively characterize the climate vulnerable regions, which could lead to more focused conservation and restoration efforts to ensure regional and global ecological safety.

As one of the most widely used schemes, the Köppen-Geiger climate classification characterizes global climate types by synthesizing annual and seasonal variations in both air temperature and precipitation (Peel et al., 2007). In addition to classifying long-term average climate, the Köppen-Geiger scheme can be used to diagnose and monitor shifts in climatic and ecosystem conditions (Chen and Chen, 2013). Numerous studies have been taken to map the recent and future global Köppen-Geiger climate zone distributions using different climate data or employing different models and scenarios (Beck et al., 2023; D. Cui et al., 2021b; Peel et al., 2007; Rohli et al., 2015a). Globally, the pace of Köppen-Geiger climate zone shifts is projected to increase approximately linearly with increasing global temperature, and about 20% of global land area undergoes climate zone shifts by the end of 21st century under RCP8.5 scenario in CMIP5 (Mahlstein et al., 2013). Notably, CMIP6 models project a higher shifting rate of climate zones due to higher warming rates than CMIP5 models, with the most pronounced changes over Europe and North America (Bayar et al., 2023). Furthermore, CMIP6 models project that 5% (SSP126 scenario) –13% (SSP585 scenario) of the global land surface will transition to a different major class (Beck et al., 2023). These findings further emphasize that global warming is the primarily factor reshaping future climate zones. However, changes in precipitation are also involved in to shape future climate zone distributions (Hamed et al., 2023), which has received less attentions. Thus, there are knowledge gaps surrounding the role of precipitation changes and interactions between precipitation and temperature changes on the redistribution of global climate zones, calling for comprehensive investigations to bridge such knowledge gaps.

In response to increasing CO_2, temperature and precipitation undergo considerable changes through CO_2 radiative effects (RAD) and reshape global climate zone distributions. Such climate zone redistributions are also contributed through vegetation physiological response (PHY) to rising CO_2. The CO_2-induced changes in vegetation biophysics, such as leaf area increase and partial stomatal closure (Ainsworth and Long, 2005; Field et al., 1995; Lammertsma et al., 2011), perturbate energy balance and influence climate. Recent studies showed that PHY amplified warming (He et al., 2022b; Park et al., 2020; Skinner et al., 2018) and enhanced seasonal temperature dynamics (He et al., 2022a). The spatial pattern of precipitation is also reshaped through PHY effects regionally and globally (J. Cui et al., 2021; Kooperman et al., 2018). However, current studies mainly investigate the PHY-induced changes in individual climate variable (temperature or precipitation), researches focusing on the overall climate change due to PHY effects are understudied. Knowledge gaps exist in how PHY affects global climate zone shifts and how it influences regional climate vulnerability, calling for thorough analyses to support climate mitigation and ecological conservation policymaking.

In this study, we quantify the Köppen-Geiger climate zone shifts with increasing atmospheric CO_2 from pre-industrial (~ 284 ppm) to 4 × CO_2 (~ 1132 ppm), and identify how PHY contributes to such shifts. We further disentangle the contributions from the PHY-induced temperature and precipitation changes, in conjunctions with their interactions, to climate zone redistributions. To accomplish these tasks, we used output from coupled Earth system model (ESM) experiments with an interactive carbon cycle from the Coupled Climate–Carbon Cycle Model Intercomparison Project (C4MIP) (Jones et al., 2016), which is endorsed by CMIP6. The effects of PHY and RAD can be isolated through the factorial simulations. Finally and most importantly, the global climate vulnerable regions are quantitatively categorized according to the gradients of CO_2-induced climate zone transitions at 4 × CO_2.

2. Materials and methods

In this study, we use the updated version of the Köppen-Geiger climate classification scheme (Beck et al., 2023; Peel et al., 2007), utilizing different thresholds of temperature and precipitation with considerations of both annual and seasonal variations (Table 1) to classify the global land surface into different climate types. Namely, five major climate zones, including tropical, arid, temperate, cold and polar zones, are defined mainly through specific thresholds of mean annual temperature (MAT) and precipitation (MAP). The second climate classes are mostly identified according to the precipitation thresholds of the driest and wettest months (Table 1). An exception is for polar zone, with the second climate classes of which are defined using temperature thresholds of the hottest month. The third level of climate category is characterized based on annual and seasonal variations in temperature. Consequently, there is a total number of 30 climate zones distributed globally based on the Köppen-Geiger climate scheme.

The Köppen-Geiger climate zone distributions are characterized using the C4MIP (Coupled Climate-Carbon Cycle Model

Table 1
Definitions of the updated Köppen-Geiger climate classifications. Adapted from Peel et al. (2007).

1st	2nd	3rd	Description	Criterion[a]
A			Tropical	Not (B) & $T_{cold} \geq 18$
	f		- Rainforest	$P_{dry} \geq 60$
	m		- Monsoon	Not (Af) & $P_{dry} \geq 100-MAP/25$
	w		- Savannah	Not (Af) & $P_{dry} < 100-MAP/25$
B			Arid	$MAP < 10 \times P_{threshold}$
	W		- Desert	$MAP < 5 \times P_{threshold}$
	S		- Steppe	$MAP \geq 5 \times P_{threshold}$
		h	- Hot	$MAT \geq 18$
		k	- Cold	$MAT < 18$
C			Temperate	Not (B) & $T_{hot} > 10$ & $0 < T_{cold} < 18$
	s		- Dry summer	$P_{sdry} < 40$ & $P_{sdry} < P_{wwet}/3$
	w		- Dry winter	$P_{wdry} < P_{swet}/10$
	f		- Without dry season	Not (Cs) or (Cw)
		a	- Hot summer	$T_{hot} \geq 22$
		b	- Warm summer	Not (a) & $T_{mon10} \geq 4$
		c	- Cold summer	Not (a or b) & $1 \leq T_{mon10} < 4$
D			Cold	Not (B) & $T_{hot} > 10$ & $T_{cold} \leq 0$
	s		- Dry summer	$P_{sdry} < 40$ & $P_{sdry} < P_{wwet}/3$
	w		- Dry winter	$P_{wdry} < P_{swet}/10$
	f		- Without dry season	Not (Ds) or (Dw)
		a	- Hot summer	$T_{hot} \geq 22$
		b	- Warm summer	Not (a) & $T_{mon10} \geq 4$
		c	- Cold summer	Not (a, b, or d)
		d	- Very cold winter	Not (a or b) & $T_{cold} < -38$
E			Polar	Not (B) & $T_{hot} \leq 10$
	T		- Tundra	$T_{hot} > 0$
	F		- Frost	$T_{hot} \leq 0$

[a] Criterion definitions: MAT–mean annual temperature; T_{cold}–the air temperature of the coldest month (°C); T_{hot}–the air temperature of the warmest month (°C); T_{mon10}–the number of months with air temperature larger than 10 °C; MAP–mean annual precipitation; P_{dry}–precipitation in the driest month (mm month^{-1}); P_{sdry}–precipitation in the driest month in summer (mm month^{-1}); P_{wdry}–precipitation in the driest month in winter (mm month^{-1}); P_{swet}–precipitation in the wettest month in summer (mm month^{-1}); P_{wwet}–precipitation in the wettest month in winter (mm month^{-1}); $P_{threshold}$–if >70% of precipitation falls in winter, $P_{threshold} = 2 \times MAT$, if >70% of precipitation falls in summer, $P_{threshold} = 2 \times MAT + 28$, otherwise $P_{threshold} = 2 \times MAT + 14$. Summer is the six-month period that is warmer between April–September and October–March, while the winter is the other six-month period.

Intercomparison Project) simulations from the idealized experiments of 1% per year cumulative increase in atmospheric CO_2 (1pctCO2), which is one of the major components joined in the C4MIP (Jones et al., 2016). The 1pctCO2 simulations employ partially coupled experiments to quantify the effects of PHY and RAD on climate and land surface (Arora et al., 2020). In detail, simulations with only land surface components experiencing increasing CO_2 (Biogeochemically coupled, named "1pctCO2-bgc") are used to monitor land surface processes changes with increasing CO_2. Simulations with only atmospheric radiation components experiencing rising CO_2 (Radiatively coupled, named "1pctCO2-rad") are used to quantify climate change in response to rising CO_2. Moreover, simulations with both atmospheric and land surface components experiencing increasing CO_2 (fully coupled, named "1pctCO2") are included to estimate coupled effects (Coupled) of rising CO_2 on both atmosphere and land surface. Additionally, we use pre-industrial simulations ("piControl") with fixing the atmospheric CO_2 at pre-industrial concentration as baseline for comparisons. In this study, we obtain outputs from nine Earth system models (ESMs) participated in CMIP6 through the data archive (https://esgf-node.llnl.gov/search/cmip6/). These ESMs include ACCESS-ESM1-5, BCC-CSM2-MR, CanESM5, CESM2, CMCC-ESM2, EC-Earth3-CC, GFDL-ESM4, IPSL-CM6A-LR and MPI-ESM1-2-LR. EC-Earth3-CC, GFDL-ESM4 and MPI-ESM1-2-LR employ dynamic vegetation models, while the remaining ESMs incorporate static vegetation modules. The monthly air temperature at 2 m and precipitation from each ESM and each factorial simulation are resampled to a common 0.5° × 0.5° grid to calculate the multi-model ensemble values. A moving window of 20 years is employed for each variable before subsequent analyses to reduce short-term fluctuations.

The Köppen-Geiger climate classification is simulated using temperature and precipitation from each ESM and each factorial simulation with atmospheric CO_2 rising from pre-industrial to 4 × CO_2. The Köppen-Geiger climate zone is also calculated using the multi-model mean of temperature and precipitation from all nine ESMs for each factorial simulation, which is regarded as the multi-model ensemble simulations of climate zone distributions. The climate zone shifts driven by rising CO_2 (Coupled) are calculated as the differences between the results of 1pctCO2 and piControl, while the effects of RAD and PHY on climate zone changes are specified using the difference of 1pctCO2 with 1pctCO2-bgc and 1pctCO2-rad, respectively. The non-linear interactions between PHY and RAD are also considered here (He et al., 2022b).

Furthermore, we conduct three factorial simulations using CMIP6 ESM outputs (Table 2) to quantify the key factors driving PHY-induced climate zone shifts with rising atmospheric CO_2. First, we conduct a control simulation (S0), utilizing PHY-induced temperature and precipitation varying with increasing CO_2 (CO_2-varying) from each CMIP6 ESM and multi-model ensemble results to calculate Köppen-Geiger climate zone distributions along the entire CO_2 gradients. The other two simulations (Table 2) are taken with only either PHY-induced precipitation (S1) or PHY-induced temperature (S2). The contributions of PHY-induced temperature (or precipitation) changes to climate zone shifts are identified by the difference between S0 and S1 (or S2). Whereas, the contributions of their interactions are characterized by the differences of the summed impacts of PHY-induced temperature and precipitation changes (S1 + S2) with the combined effects (S0). The results of key drivers for PHY-induced climate shifts at 4 × CO_2 are illustrated spatially across each IPCC AR6 climate reference land region (Iturbide et al., 2020). At the same time, dominant factors for the pace of climate zone shifts are identified across the full range of atmospheric CO_2.

Finally, we categorize global vulnerable regions based on the extent of climate zone shifts induced through CO_2 Coupled effects and into three levels. The strong climate vulnerable regions (Vulnerability = 3) are defined as regions experiencing major climate zone changes, such as shifting from temperate to tropical zones. Regions undergoing transitions between second climate categories, such as transitioning from BSh (arid, steppe, hot) to BWh (arid, desert, hot), are classified as moderate vulnerable regions (Vulnerability = 2). Whereas, minor vulnerable regions (Vulnerability = 1) are defined over those regions facing climate zones changes within the third classification categories, such as changing from Dfc (cold, no dry season, cold summer) to Dfb (cold, no dry season, warm summer).

3. Results

3.1. Global climate zone shifts from pre-industrial to 4 × CO_2

At pre-industrial CO_2 concentration (~ 284 ppm), tropical savannah (Aw) has the largest areas (14.2% of global land surface), and is mainly located in the South America, Central Africa and South Asia (Fig. 1a). BWh (arid, desert, hot) is the second largest, with a total distribution of 1.81×10^7 km^2 (~13.6% of global land area), and is mostly found in the Sahara Desert. In the northern high latitudes, Dfc (cold, no dry season, cold summer) is the most common climate type, accounting for about 12.6% of global land area. However, diverse climate types are shown in

Table 2
Summary of factorial simulations with vegetation physiological responses to increasing CO_2 (PHY).

Scenarios	PHY-induced Temperature	PHY-induced Precipitation
S0	Varying with increasing CO_2	Varying with increasing CO_2
S1	Fixed at pre-industrial CO_2 level	Varying with increasing CO_2
S2	Varying with increasing CO_2	Fixed at pre-industrial CO_2 level

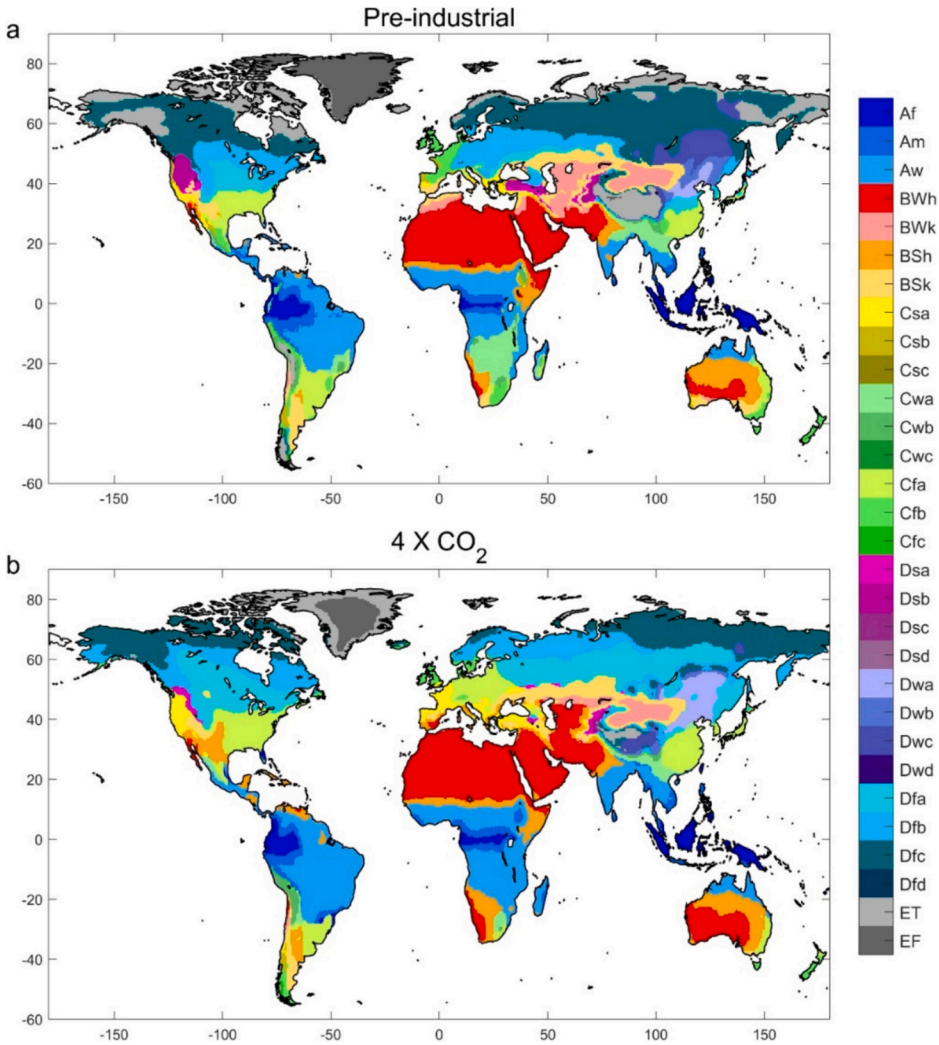

Fig. 1. Global distributions of Köppen-Geiger climate zones with atmospheric CO_2 concentration at pre-industrial (a) and 4 × CO_2 (b). Note, (b) shows the results from coupled CO_2 effects at 4 × CO_2.

the northern mid-latitudes, spanning from cold to arid zones (Fig. 1a). The spatial distributions of these climate zones reflect the regional characteristics of precipitation and temperature and their variations at pre-industrial CO_2 concentration.

As atmospheric CO_2 rises to quadruple levels, changes in precipitation and temperature dramatically reshape the global patterns of climate zones (Fig. 1b). Over half of the global land area experiences climate zone shifts due to increasing atmospheric CO_2. Such shifts are mostly

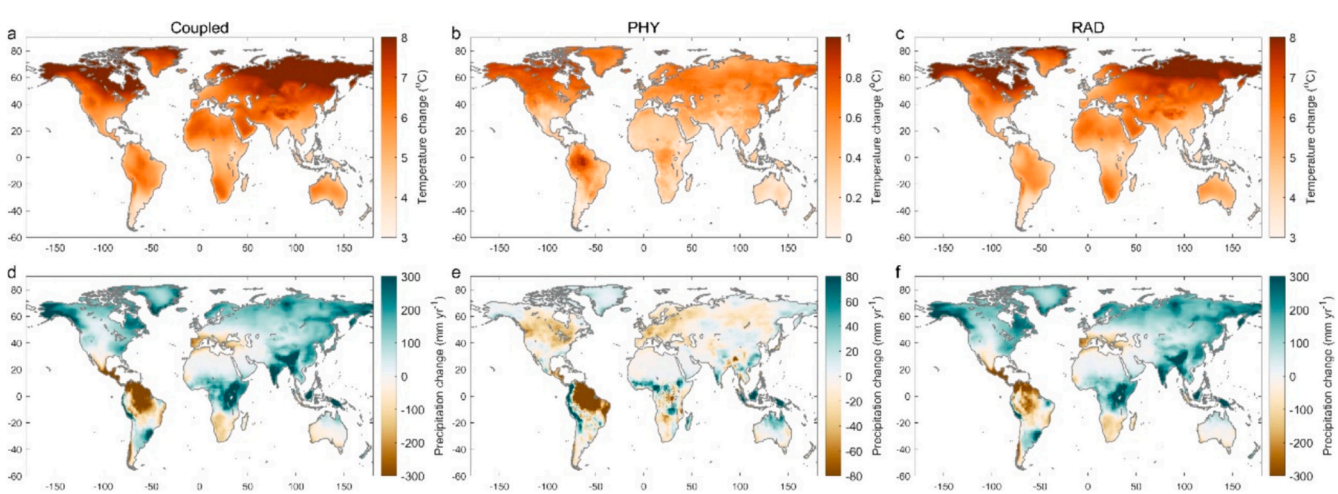

Fig. 2. CO_2-induced changes in temperature and precipitation at 4 × CO_2. Changes in temperature (a-c) and precipitation (d-f) driven by effects of CO_2 (Coupled; a, d), vegetation physiological forcing (PHY; b, e) and radiative forcing (RAD; c, f) at 4 × CO_2, respectively.

found in the northern high latitudes (Fig. 1b), where considerable temperature and precipitation increase (Fig. 2) tends to shift the local climate zone from Dfc to Dfb (cold with no dry season and warm summer) and Dfa (cold with no dry season and hot summer) (Fig. 3a). In contrast, The ET (polar tundra) climate zone retreats by more than half (~ 52.8%) of its coverage at pre-industrial CO_2 level to Dfc at 4 × CO_2, which is shown in both northern high latitudes and the Tibetan Plateau (Fig. 1b). As a result, Dfc experiences the most dramatic changes in response to rising CO_2, with a net area decrease of 45.9% of its pre-industrial coverage and only covering about 6.8% of global land area at 4 × CO_2. Owing to the transitions from Dfc, Dfa has the largest area expansions (Fig. 3a), and finally distributes across about 9.4% (1.25 × 10^7 km^2) of global land area at 4 × CO_2. Such area expansions of Dfa are also contributed (~ 41.1%) by shifts from Dfb. It is worth noting that ET climate zone in the Tibetan Plateau (Fig. 1b) is mainly converted to Dwc (cold with dry winter and cold summer). Another strong signal is that the arid regions, especially BWh, show northward expansions responding to 4 × CO_2 (Fig. 1b), with the coverage increasing by about 24.4% of its pre-industrial level. Moreover, BSh (arid, steppe and hot) is expanding mainly at the expense of BSk (arid, steppe and cold), Aw and Cfa (temperate, no dry season, hot summer), due to increased temperature and reduced precipitation (Fig. 2) through coupled effects of 4 × CO_2 (Fig. 3a).

Simultaneously, several other climate zones also undergo shifts in response to 4 × CO_2. Specifically, Aw shows prominent poleward migrations globally. Particularly, in the south Africa, the local climate shifts from Cwa (temperate, dry winter and hot summer) to Aw (Fig. 1b), which is also the case for south Asia. The distribution of Aw is also expanded from Am (tropical monsoon) in the Amazon rainforests due to CO_2-induced precipitation reduction (Fig. 2d). Overall, the global distributions of climate zones are reshaped considerably in response to 4 × CO_2. Generally, tropical and arid zones experience remarkable expansions (Fig. S1), while temperate, cold and polar zones undergo large shrinkage at 4 × CO_2, especially for polar zones, retreating about 71.4% of their pre-industrial coverage (6.3% of global land area).

3.2. Role of PHY to shift global climate zones at 4 × CO_2

To dig into the mechanisms behind the climate zone shifts, we investigate the effects from PHY and RAD on the global climate zone changes. Although RAD forces climate zone shift over a vast area (Fig. 3c) and is already well studied (D. Cui et al., 2021a; Mahlstein et al., 2013; Rohli et al., 2015a; Skalák et al., 2018), PHY redistributes climate zone across nearly 9.5% of the global land area, accounting for about 16.8% of Coupled-induced climate zone shifts at 4 × CO_2. PHY induces strong shrinkages in the distributions of cold zones due to amplified warming (Fig. 2b), occupying 9.1% of Coupled-induced area changes in cold zones at 4 × CO_2 (Fig. S1). In detail, a large proportion of cold zones (i.e. Dfa and Dfb) is shifted to BSk and Cfa, whereas, substantial transitions are also found between different cold zones induced by PHY effects (Fig. 3b). Typically, PHY triggers considerable area increases in Dfa at 4 × CO_2 (Fig. S2), mainly at the expense of Dfb over the northern mid-latitudes (Fig. S3a), and accounts for about 32.8% of area increases by CO_2 Coupled effects. However, Dfb gains area from Dfc as PHY drives 9.6% of Dfc pre-industrial coverage to be Dfb at 4 × CO_2 (Fig. 3b). Therefore, PHY causes Dfb shrinkage (−15.3%) at 4 × CO_2, which is also contributed by shifting to drier (i.e. Dwb: cold, dry winter, warm summer) and warmer (i.e. Cfb: temperate, no dry season, warm summer) classifications. In addition, PHY drives area increase in Dwa (cold, dry winter, hot summer), occupying about 11.9% of that through Coupled effects at 4 × CO_2. As a result, PHY ultimately diminishes the distributions of cold zone at 4 × CO_2.

Interestingly, PHY poses effects to promote aridification at 4 × CO_2, contributing about 4.2% of the total arid zone area increases through Coupled effects. Such PHY-facilitated aridification is mostly shifted from tropical and temperate zones under pre-industrial climate (Fig. S1b). Specifically, PHY-induced expansions of BWh dominate the PHY-triggered aridification at 4 × CO_2 (Fig. 3b), and contribute about 10.3% of its area increases through CO_2 Coupled effects. Although PHY triggers substantial shifts from Aw to BSh (Fig. 3b), mainly located in the northeast South America, about two-thirds of such shifts are returned back (BSh to Aw) in central Africa and India (Fig. S3a). Generally, due to PHY-induced temperature increase (Fig. 2b) and precipitation reduction (Fig. 2e), PHY shifts the climate zones from BWk (arid, desert, cold), BSh and BSk to BWh (Fig. 3b), which are mostly located over northwest Africa and southwest Australia.

Nevertheless, PHY contributes to further northward migrations of tropical zones at 4 × CO_2 (Fig. 3b). Although some regions in the northeast Amazon and southern Sahara (Fig. S3a) experience climate shifts from Aw to BSh, shifts from BSh, Cfa, Cwa, and Cwb (temperate, dry winter and warm summer) add 30% more area to broaden the distributions of tropical zones. Additionally, evident polar zone retreats are shown through PHY effects at 4 × CO_2, about 90% of which is converted to cold zones (Fig. 3b).

To better understand the underlying mechanisms driving PHY-induced climate zone shifts, we further attribute such shifts to changes in temperature, precipitation, and their interactions across each IPCC AR6 reference land region (Fig. 4) and along the full gradients of atmospheric CO_2 concentration (Fig. 5). As CO_2 rises to quadruple levels, PHY-induced temperature enhancements dominate the associated climate zone shifts over 54.5% of the AR6 land regions, spanning from high to middle latitudes in both hemisphere (Fig. 4a). Importantly, the

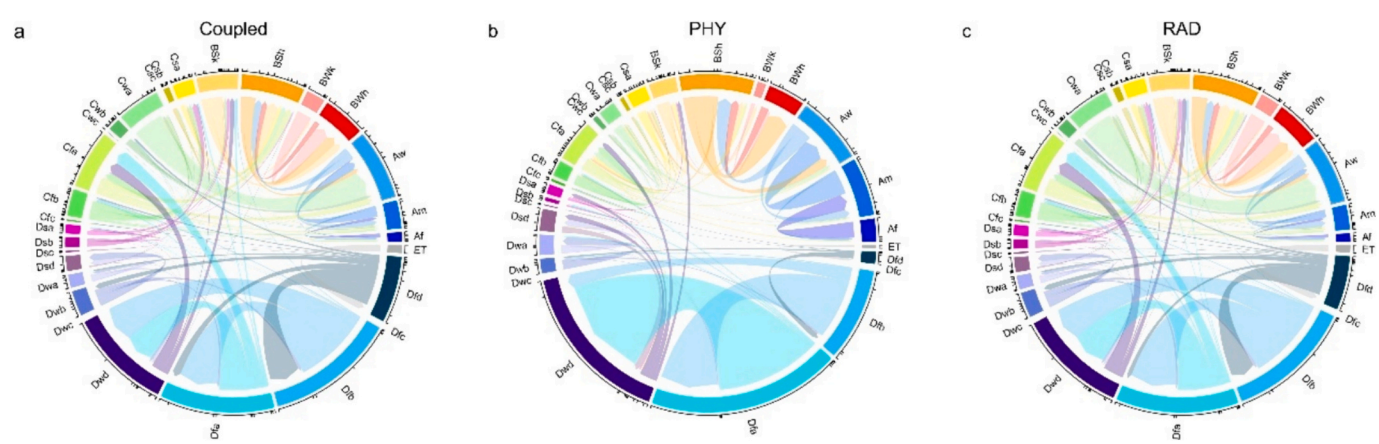

Fig. 3. Global transitions among different Köppen-Geiger climate zones at 4 × CO_2. Climate zone area changes due to the effects of CO_2 (a; Coupled), physiological (b; PHY) and radiative (c; RAD) forcings responding to 4 × CO_2.

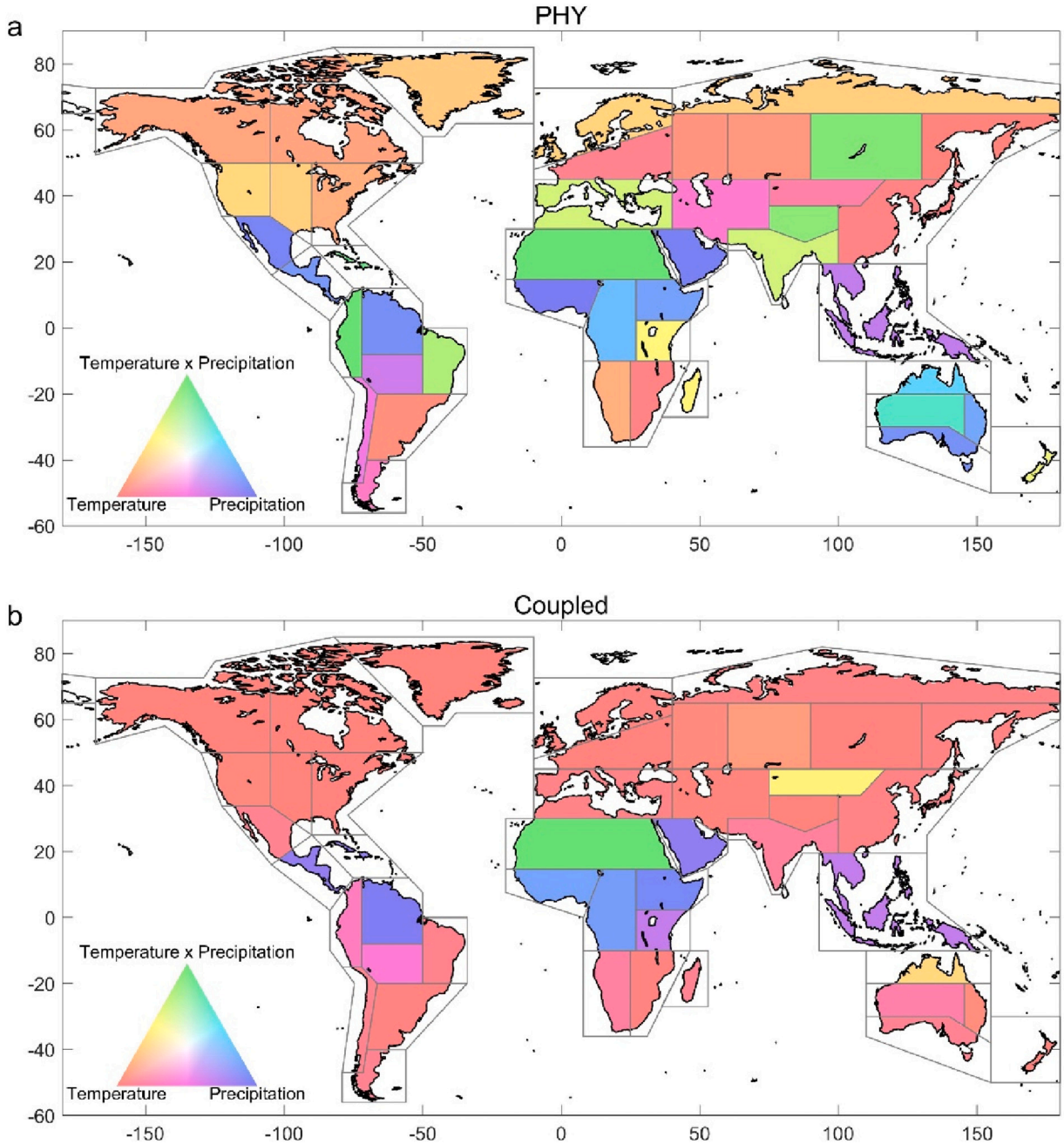

Fig. 4. Key factors driving CO_2-induced climate zone shifts at 4 × CO_2 globally. The dominant factors for climate zone shift driven by vegetation physiological response (PHY; a) and coupled effects (Coupled; b) at 4 × CO_2 for each AR6 reference region are shown. The specific contributions from temperature change, precipitation change and their interactions (Temperature × Precipitation) through PHY and Coupled effects are identified.

interactions between temperature and precipitation changes under PHY show dominance for climate shifts over 15.9% of all the AR6 reference land regions at 4 × CO_2, such as East Siberia (ESB; Fig. S4) and North East South America (NES). Climate zone changes across the rest regions are dominated by PHY-induced precipitation changes (Fig. 2e), particularly in North Central America (NCA), North South America (NSA) and North Eastern Africa (NEAF). Therefore, PHY-forced temperature increase is the primary factor driving the corresponding climate zone to shift to warmer and drier classifications at 4 × CO_2.

The pace of changes in each climate zone area induced by PHY effects is analyzed with increasing atmospheric CO_2 (Fig. 5), including both area gains from and losses to other climate zones. With increasing atmospheric CO_2, PHY drives continuous area changes across 23 climate zones, due to the induced changes in temperature, precipitation and their interactions. Critically, PHY forces 56.7% of climate zones to shift faster with rising CO_2, indicated by significant positive trends in area changes of those zones (Fig. 5a). Three cold zones, including Dfa, Dfb, and Dfc, show obviously larger positive trends with rising CO_2 than other ones by PHY effects, ranging from 2.44×10^3 (Dfc) to 5.56×10^3 (Dfb) km^2 ppm^{-1} (Fig. 5a). Particularly, PHY drives substantial shifts between Dfb and Dfc, as well as Dfa and Dfb, leading to diminished distributions of Dfb and Dfc, and expansions of Dfa as CO_2 approaches quadruple levels. PHY forces temperature in those three zones to continuously increase with rising CO_2 (Fig. 5b), and dominantly promotes climate shifts from Dfc to Dfb (Fig. 5d). Manipulated by the interactions (Fig. 5d) between PHY-driven temperature increases (Fig. 5b) and precipitation reductions (Fig. 5c), Dfa is mostly converted to Dwa and Cfa (Fig. 3b). Thus, PHY-induced temperature enhancements, in

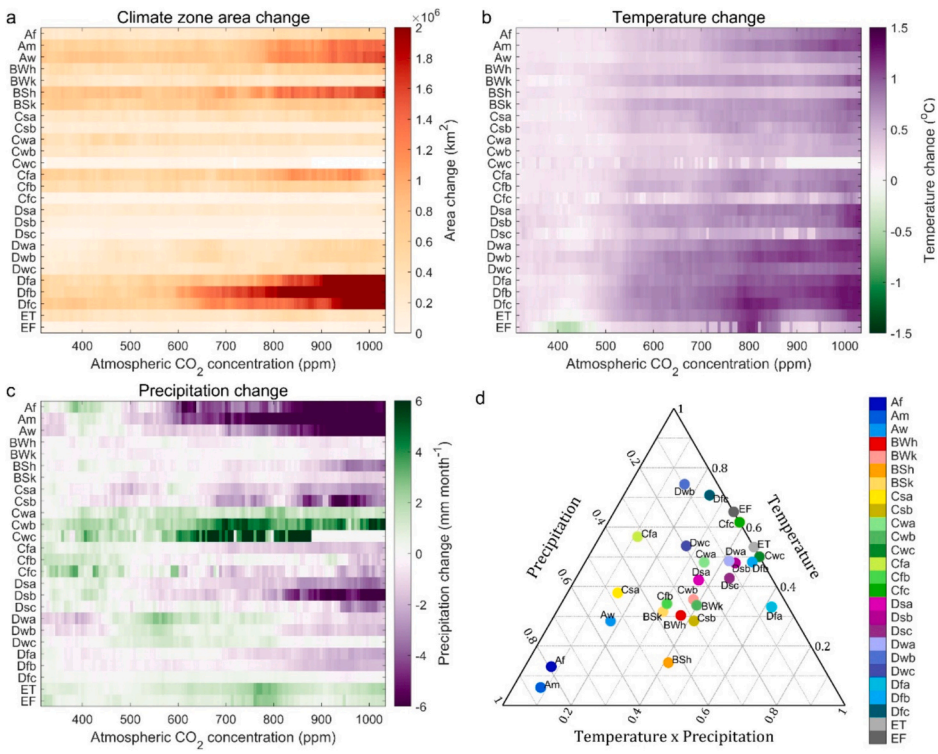

Fig. 5. Pace of changes in each climate zone driven by vegetation physiological response to increasing CO_2. (a) The area changes of each climate zone with rising CO_2 from pre-industrial to 4 × CO_2 driven by vegetation physiological forcing (PHY), including area gains from and losses to other climate types. (b) PHY-induced temperature change for each climate zone along the gradients of atmospheric CO_2. (c) PHY-induced precipitation changes in response to increasing CO_2 for each climate zone. (d) Attributions of PHY-induced climate zone area changes to temperature change, precipitation change and their interactions for each climate zone with increasing CO_2.

conjunction with their interactions with precipitation changes, are the dominant factors driving the transitions between above three cold zones in response to rising CO_2.

It is worth noting that Aw and BWh are the two most widely distributed climate zones globally at pre-industrial CO_2 concentration (Fig. 1a). They both experience continuously significant expansions through PHY effects with increasing CO_2, and achieve final distributions of 2.04×10^7 (15.4% of the global land area) and 1.83×10^7 (13.8%) km^2, respectively, maintaining to be the first and second largest distributed climate zone globally, which is also true for Coupled results (Fig. 1b). Such continuous expansions are primarily driven by PHY-induced precipitation changes and their interactions with PHY-induced temperature increase, respectively (Fig. 5d).

In contrast, the area changes of six climate zones, including Csb (temperate, dry summer, warm summer), Cwa, Cwb, Cwc (temperate, dry winter, cold summer), Dsb (cold, dry summer, warm summer) and Dsc (cold, dry summer, cold summer), significantly level off through PHY effects, though their negative trends are relatively small (Fig. 5a). These shifts in Cwa, Cwc and Dsb are primarily driven by PHY-induced temperature increase, whereas, shifts in the rest three climate zones are mainly due to the interactions of PHY-induced temperature and precipitation changes (Fig. 5d). Governed by PHY-induced temperature and precipitation increase, Cwb suffers from the strongest decline trend with a rate of -2.54×10^2 km^2 ppm^{-1} (Fig. 5a), resulting in a final distribution of 1.38×10^6 km^2 at 4 × CO_2. Comparatively, there are also some climate zones (i.e. BWk) experiencing drastic changes with increasing atmospheric CO_2 (Fig. 5a), resulting in non-significant trends of area changes across the full range of atmospheric CO_2. These are mostly due to the considerable interactions between PHY-forced temperature and precipitation changes (Fig. 5d). Consequently, forced by PHY effects, the increased temperature dominates about 46.2% of climate zone transitions from pre-industrial to 4 × CO_2, while the rest ones are caused by the corresponding precipitation changes (26.9%) and their interactions (26.9%) with temperature changes.

In summary, PHY contributes 16.8% of total climate zone shifts and accounts for about 9.1% of the cold zone shrinkage and 4.2% of arid zone expansions induced by Coupled effects at 4 × CO_2 (Fig. 1). Furthermore, PHY drives continuously significant area increases in 17 climate zones and area reductions in six zones with increasing CO_2 (Fig. 5), suggesting that the crucial importance of vegetation feedbacks in climate zone redistributions with rising CO_2 should not be overlooked. Such PHY-induced climate shifts are mainly driven by temperature amplification through PHY over about half of the land regions. However, precipitation changes and the associated interactions with temperature changes show dominance over the rest regions.

3.3. Assessment of global climate zone vulnerability

The global climate zone shifts show considerable spatial heterogeneity at 4 × CO_2 (Fig. 6), which indicate that different regions might face different level of climate vulnerability to influence local ecosystem structure and function, calling for different efforts for ecological conservation and restoration. Thus, the global land area is categorized into three vulnerability classes depending on the extent of climate zone shifts induced by Coupled effects at 4 × CO_2, ranging from strong (Vulnerability = 3) to minor vulnerability (Vulnerability = 1). Surprisingly, 22.0% of the global land area experiences the shifts between major climate zones (Vulnerability = 3), and 5.7% of such shifts are contributed by PHY effects at 4 × CO_2 (Fig. 6). Generally, in the Northern Hemisphere, the local climate shifts from polar to cold zones over high latitudes and Tibetan Plateau, and from cold to temperate zones over mid-latitudes for those strong climate vulnerable regions (Fig. 1). Whereas, the strong vulnerable regions in the Southern Hemisphere (Fig. 6) mostly exhibit shifts from temperate to tropical climate zones,

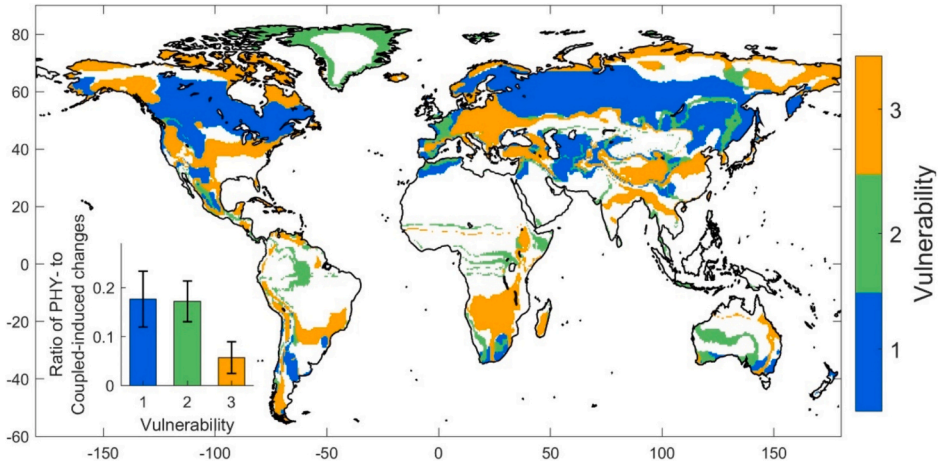

Fig. 6. Global characterization of vulnerability at 4 × CO_2. Global vulnerable regions are categorized according to the extent of climate zone shifts driven by quadruple CO_2, suggesting strong vulnerable regions (Vulnerability = 3) experiencing major climate zone shifts, moderate vulnerable regions (Vulnerability = 2) undergoing shifts between sub-major classes, and minor vulnerable regions (Vulnerability = 1) facing climate shifts between third-level categories. The contributions from PHY effects are shown in the lower left insert plot.

illustrating the emergence of more severe climate shifts in the Southern Hemisphere than Northern Hemisphere. Those severe changes are primarily driven by CO_2-induced temperature amplifications (Fig. 4b), 5.6% of which is contributed by PHY effects in response to 4 × CO_2.

Moreover, the regions suffer from moderate climate vulnerability (Vulnerability = 2) is only distributed across 9.1% of global land area at 4 × CO_2, 17.2% of which is contributed by PHY effects (Fig. 6). The corresponding climate zone shifts mostly happen between different temperate zones in the Northern Hemisphere, dominated by CO_2-induced warming (Fig. 4b). However, CO_2-triggered precipitation changes are involved to influence the transitions between different tropical zones in South America, and dominate the shifts between different arid zones in Australia. The regions facing minor climate vulnerability (Vulnerability = 1) can be found over more than one-fifth of global land surface (Fig. 6), the majority of which are located in the northern mid-to-high latitudes associated with shifts from Dfc to Dfb and Dfa (Fig. 1). Across these regions, PHY triggers significant temperature increase (He et al., 2022b), and contributes about 17.6% to convert local climate to warmer ones.

4. Discussion and conclusions

Using nine ESMs from the CO_2-forcing experiments in the CMIP6-endorsed C4MIP, our results show that about 51.2% of the global land area experiences climate zone changes due to the Coupled effects from pre-industrial to 4 × CO_2, generally shifting to warmer and drier classifications (Fig. 1). These results are very close to the results from a previous study indicating that about 48.0% of global land area faced climate zone changes under the SSP585 scenario according to the CMIP6 projections (Bayar et al., 2023). However, the results from the CMIP5 RCP8.5 scenario show that about 37.9% of global land area would experience climate zone changes by the end of this century, which are slightly lower than that from CMIP6 simulations due to lower warming rates (Bayar et al., 2023). We find that tropical and arid climates expand and polar zones shrink in response to rising CO_2, supporting previous findings using CMIP5 results (Crosbie et al., 2012; D. Cui et al., 2021a; Rohli et al., 2015a; Wu et al., 2021). The hotter and drier subtypes in arid and temperate classifications show expansions in Central Asia under different scenarios (RCP2.6, RCP4.5 and RCP8.5) in CMIP5 simulations (He et al., 2021), which are also shown in our results (Fig. 1). The major climate zone shifts in Southeast Asia are mainly due to increased precipitation in the wet season under different scenarios in CMIP6 (Hamed et al., 2023), supporting our results (Fig. 4).

Using data from 67 ESMs, a recent study (Beck et al., 2023) stated that about 13% of the land surface would suffer from climate zone shifts to a different major class (strong vulnerability) under the SSP585 scenario in CMIP6 from 1991–2020 to 2071–2099. However, our study illustrates that with atmospheric CO_2 rising from pre-industrial to quadruple levels, such proportion would be increased to 22.0%. Although discrepancies exist when using different climate products (Hobbi et al., 2022), most of the ESMs used in this study share generally strong agreements in climate zone delineations and changes from pre-industrial to 4 × CO_2 (Fig. S5), suggesting that our results are robust with respect to the nine ESMs used in this study. However, models exhibit relatively higher agreements at pre-industrial level than 4 × CO_2, especially in Eurasia (Fig. S5), possibly introducing biases in projecting climate zone redistributions in these regions at 4 × CO_2. In addition, relatively low agreements are shown in permafrost regions (northern high latitudes and Tibet Plateau) due to inadequate representations of permafrost processes in current ESMs (Schädel et al., 2024). Hence, more field measurements and efforts are imperative to better constrain models and improve projections in future climate zone shifts across those permafrost regions. Model simulations with fine resolution are also promising solutions for improving the characterization of Köppen-Geiger climate zone shifts (Guan et al., 2021).

Global warming with increasing atmospheric CO_2 are identified as the dominant factor driving climate zone shifts in most cases, projecting larger shifting rates under stronger warming (Bayar et al., 2023; Beck et al., 2023; Mahlstein et al., 2013). However, precipitation changes also influence climate zone shifts (Hamed et al., 2023), especially vegetation change-induced precipitation changes (Cui et al., 2020; Kooperman et al., 2018). Spatially, we show that PHY-induced precipitation changes and the associated interactions with temperature change has a leading role in driving climate zone transitions over 45.5% of the global land area at 4 × CO_2 (Fig. 4). In terms of pace of climate zone area changes with rising CO_2, precipitation changes and associated interactions with temperature changes are the main contributors to about 53.8% of global climate zone shifts (Fig. 5). It is well-known that climate plays a dominant role in vegetation distributions across the land surface, however, how land-surface vegetation change modulates regional climate remain poorly understood. Previous studies showed that through CO_2-induced leaf area increase and partial stomata closure, PHY continuously amplifies warming and enhanced temperature season dynamics with increasing CO_2 (He et al., 2022a, 2022b). In addition, precipitation patterns were also shown to experience substantial changes through PHY effects in previous studies, mainly due to reduced

evapotranspiration through partial stomatal closure (Betts et al., 2007; J. Cui et al., 2021). In contrast to previous studies that only focused on the individual identification of either temperature or precipitation change in response to increasing CO_2, our findings indicate that vegetation response to rising CO_2 plays a critical role in reshaping the overall climate in terms of both temperature and precipitation changes. The characterization of key factors by PHY deepens our understanding of climate zone shifts with increasing CO_2, providing new perspectives on climate-vegetation interactions. The insights gained from our analyses also help model improvements for future projections of climate and vegetation distributions.

At $4 \times CO_2$, more than one-fifth of global land area suffer from strong climate vulnerability, as the local climate shifts to a different major type (Fig. 6). Notably, regions with strong climate vulnerability generally shift from temperate to tropical zones in the Southern Hemisphere, whereas, they change from polar to cold or cold to temperate zones in the Northern Hemisphere. Consequently, although sharing the same level of climate vulnerability, regions in the Southern Hemisphere are more vulnerable than those in the Northern Hemisphere, suggesting that ecosystems and human society there will face more risks and threats at $4 \times CO_2$ and more efforts are required there to mitigate climate change. The CO_2-induced precipitation reductions over those regions of the Southern Hemisphere (Fig. 2d) might lead to water scarcity to influence both vegetation growth and human living. Effective water conservation strategies are in high priority there. Moreover, rising CO_2 induces warming in those regions at $4 \times CO_2$, which may lead to exceedance of the optimum temperature for vegetation photosynthesis (Huang et al., 2019), resulting in tree mortality and ecosystem function loss. It is also worth noting that the most vulnerable regions in the Northern Hemisphere are generally densely populated, and dramatic climate zone shifts occurring there will pose considerable threats to human society (Malone, 2023), prompting the need for further assessments on population exposure to climate shifts with increasing CO_2.

The case is quite different for regions experiencing minor vulnerability, mainly located in northern mid-to-high latitudes (Fig. 6). Climate zone shifts there might impose positive impacts on ecosystem structure and function, as CO_2-enhanced temperature increase promotes growth of boreal forests through extending growing season and enhancing photosynthesis (Zhu et al., 2016). However, those regions (Vulnerability = 1) may face threats of climate extremes, suffering from earlier drought (Zhang and Gao, 2023), heatwave and even wildfire (Gloege et al., 2022; Webb et al., 2024) with higher frequency and severity at $4 \times CO_2$. Furthermore, historical agriculture land may become less suitable for certain crops and irrigation demand might face threats due to climate zone shifts, requiring adjustments in farming practice to ensure food security. Therefore, by identifying climate vulnerable regions at $4 \times CO_2$, we can prioritize conservation and restoration efforts to those areas, providing scientific insights to support climate mitigation and adaptation.

In summary, our study demonstrates widespread shifts of global climate zone in response to increasing atmospheric CO_2 in which vegetation physiological response (PHY) plays a non-negligible role on these shifts. We find that 51.2% of the global land surface suffers from increased vulnerability due to CO_2-induced climate zone shifts, 16.8% of which is contributed by PHY effects. Unraveling the effects of temperature change, precipitation change and their interactions, PHY considerably contributes to poleward extensions of tropical and temperate zones, expansions of arid zone and retreats of polar zones, deepening our knowledge on future climate zone distributions and promoting future projections of climate and vegetation dynamics. Our study emphasizes the urgency to reduce ecological and hydrological vulnerability and enhance adaptive capacity of targeted regions, ensuring tailored conservation efforts and policies to meet specific needs and pressing challenges of different vulnerable regions.

CRediT authorship contribution statement

Mingzhu He: Writing – original draft, Visualization, Methodology, Funding acquisition, Formal analysis, Data curation, Conceptualization. **Jiangpeng Cui:** Writing – review & editing, Methodology, Conceptualization. **Yonghong Yi:** Writing – review & editing, Methodology, Conceptualization. **Hans W. Chen:** Writing – review & editing. **Qian Zhang:** Writing – review & editing. **Lili Li:** Writing – review & editing. **Ling Huang:** Writing – review & editing. **Songbai Hong:** Writing – review & editing.

Declaration of competing interest

The authors declare no competing interests.

Data availability

All data sets and materials used in this study are freely available online: https://esgf-node.llnl.gov/search/cmip6/.

Acknowledgement

This study was supported by the National Natural Science Foundation of China (grant number 52394232), "the Fundamental Research Funds for the Central Universities" and Beijing Normal University Project (grant number 03700-312223501501). The work was also partly funded by the International Science and Technology Cooperation Program under the 2023 Shanghai Action Plan for Science, Technology and Innovation [grant number 23230712800].

Appendix A. Supplementary data

Supplementary data to this article can be found online at https://doi.org/10.1016/j.scitotenv.2024.174810.

References

Ainsworth, E.A., Long, S.P., 2005. What have we learned from 15 years of free-air CO_2 enrichment (FACE)? A meta-analytic review of the responses of photosynthesis, canopy properties and plant production to rising CO_2. New Phytol. 165, 351–372. https://doi.org/10.1111/j.1469-8137.2004.01224.x.

Arora, V.K., Katavouta, A., Williams, R.G., Jones, C.D., Brovkin, V., Friedlingstein, P., Schwinger, J., Bopp, L., Boucher, O., Cadule, P., Chamberlain, M.A., Christian, J.R., Delire, C., Fisher, R.A., Hajima, T., Ilyina, T., Joetzjer, E., Kawamiya, M., Koven, C. D., Krasting, J.P., Law, R.M., Lawrence, D.M., Lenton, A., Lindsay, K., Pongratz, J., Raddatz, T., Séférian, R., Tachiiri, K., Tjiputra, J.F., Wiltshire, A., Wu, T., Ziehn, T., 2020. Carbon–concentration and carbon–climate feedbacks in CMIP6 models and their comparison to CMIP5 models. Biogeosciences 17, 4173–4222. https://doi.org/10.5194/bg-17-4173-2020.

Bayar, A.S., Yılmaz, M.T., Yücel, İ., Dirmeyer, P., 2023. CMIP6 earth system models project greater acceleration of climate zone change due to stronger warming rates. Earth's Futur. 11, e2022EF002972 https://doi.org/10.1029/2022EF002972.

Beck, H.E., McVicar, T.R., Vergopolan, N., Berg, A., Lutsko, N.J., Dufour, A., Zeng, Z., Jiang, X., van Dijk, A.I.J.M., Miralles, D.G., 2023. High-resolution (1 km) Köppen-Geiger maps for 1901–2099 based on constrained CMIP6 projections. Sci. Data 10, 724. https://doi.org/10.1038/s41597-023-02549-6.

Betts, R.A., Boucher, O., Collins, M., Cox, P.M., Falloon, P.D., Gedney, N., Hemming, D. L., Huntingford, C., Jones, C.D., Sexton, D.M.H., Webb, M.J., 2007. Projected increase in continental runoff due to plant responses to increasing carbon dioxide. Nature 448, 1037–1041. https://doi.org/10.1038/nature06045.

Chen, D., Chen, H.W., 2013. Using the Köppen classification to quantify climate variation and change: an example for 1901–2010. Environ. Dev. 6, 69–79. https://doi.org/10.1016/j.envdev.2013.03.007.

Chen, I.-C., Hill, J.K., Ohlemüller, R., Roy, D.B., Thomas, C.D., 2011. Rapid range shifts of species associated with high levels of climate warming. Science 80-.). 333, 1024–1026. https://doi.org/10.1126/science.1206432.

Crosbie, R.S., Pollock, D.W., Mpelasoka, F.S., Barron, O.V., Charles, S.P., Donn, M.J., 2012. Changes in Köppen-Geiger climate types under a future climate for Australia: hydro- logical implications. Hydrol. Earth Syst. Sci. 16, 3341–3349. https://doi.org/10.5194/hess-16-3341-2012.

Cui, J., Piao, S., Huntingford, C., Wang, X., Lian, X., Chevuturi, A., Turner, A.G., Kooperman, G.J., 2020. Vegetation forcing modulates global land monsoon and water resources in a CO_2-enriched climate. Nat. Commun. 11, 5184. https://doi.org/10.1038/s41467-020-18992-7.

Cui, J., Yang, H., Huntingford, C., Kooperman, G.J., Lian, X., He, M., Piao, S., 2021. Vegetation response to rising CO_2 amplifies contrasts in water resources between global wet and dry land areas. Geophys. Res. Lett. 48, e2021GL094293 https://doi.org/10.1029/2021GL094293.

Cui, D., Liang, S., Wang, D., 2021a. Observed and projected changes in global climate zones based on Köppen climate classification. WIREs Clim. Chang. 12, e701 https://doi.org/10.1002/wcc.701.

Cui, D., Liang, S., Wang, D., Liu, Z., 2021b. A 1 km global dataset of historical (1979–2013) and future (2020−2100) Köppen–Geiger climate classification and bioclimatic variables. Earth Syst. Sci. Data 13, 5087–5114. https://doi.org/10.5194/essd-13-5087-2021.

Field, C.B., Jackson, R.B., Mooney, H.A., 1995. Stomatal responses to increased CO_2: implications from the plant to the global scale. Plant Cell Environ. 18, 1214–1225. https://doi.org/10.1111/j.1365-3040.1995.tb00630.x.

Gibson, A.J., Hancock, G.R., Verdon-Kidd, D.C., Martinez, C., Wells, T., 2021. The impact of shifting Köppen-Geiger climate zones on soil organic carbon concentrations in Australian grasslands. Glob. Planet. Change 202, 103523. https://doi.org/10.1016/j.gloplacha.2021.103523.

Gloege, L., Kornhuber, K., Skulovich, O., Pal, I., Zhou, S., Ciais, P., Gentine, P., 2022. Land-atmosphere cascade fueled the 2020 Siberian heatwave. AGU Adv. 3, e2021AV000619. https://doi.org/10.1029/2021AV000619.

Guan, Y., Cui, W., Liu, J., Lu, H., Jiang, Y., Xue, Y., Heiskanen, J., 2021. Observed changes of Köppen climate zones based on high-resolution data sets in the Qinghai-Tibet Plateau. Geophys. Res. Lett. 48, 1–9. https://doi.org/10.1029/2021GL096159.

Hamed, M.M., Nashwan, M.S., Shahid, S., Wang, X.-J., Ismail, T. Bin, Dewan, A., Asaduzzaman, M., 2023. Future Köppen-Geiger climate zones over Southeast Asia using CMIP6 multimodel ensemble. Atmos. Res. 283, 106560 https://doi.org/10.1016/j.atmosres.2022.106560.

He, H., Luo, G., Cai, P., Hamdi, R., Termonia, P., De Maeyer, P., Kurban, A., Li, J., 2021. Assessment of climate change in Central Asia from 1980 to 2100 using the Köppen-Geiger climate classification. Atmosphere (Basel). 12, 123. https://doi.org/10.3390/atmos12010123.

He, M., Lian, X., Cui, J., Xu, H., Piao, S., 2022a. Vegetation physiological response to increasing atmospheric CO_2 slows the decreases in the seasonal amplitude of Temperature. Geophys. Res. Lett. 49, 1–8. https://doi.org/10.1029/2022GL097829.

He, M., Piao, S., Huntingford, C., Xu, H., Wang, X., Bastos, A., Cui, J., Gasser, T., 2022b. Amplified warming from physiological responses to carbon dioxide reduces the potential of vegetation for climate change mitigation. Commun. Earth Environ. 3, 160. https://doi.org/10.1038/s43247-022-00489-4.

Hobbi, S., Michael Papalexiou, S., Rupa Rajulapati, C., Nerantzaki, S.D., Markonis, Y., Tang, G., Clark, M.P., 2022. Detailed investigation of discrepancies in Köppen-Geiger climate classification using seven global gridded products. J. Hydrol. 612, 128121 https://doi.org/10.1016/j.jhydrol.2022.128121.

Huang, M., Piao, S., Ciais, P., Peñuelas, J., Wang, X., Keenan, T.F., Peng, S., Berry, J.A., Wang, K., Mao, J., Alkama, R., Cescatti, A., Cuntz, M., De Deurwaerder, H., Gao, M., He, Y., Liu, Y., Luo, Y., Myneni, R.B., Niu, S., Shi, X., Yuan, W., Verbeeck, H., Wang, T., Wu, J., Janssens, I.A., 2019. Air temperature optima of vegetation productivity across global biomes. Nat. Ecol. Evol. 3, 772–779. https://doi.org/10.1038/s41559-019-0838-x.

Iturbide, M., Gutiérrez, J.M., Alves, L.M., Bedia, J., Cerezo-Mota, R., Cimadevilla, E., Cofiño, A.S., Di Luca, A., Faria, S.H., Gorodetskaya, I.V., Hauser, M., Herrera, S., Hennessy, K., Hewitt, H.T., Jones, R.G., Krakovska, S., Manzanas, R., Martínez-Castro, D., Narisma, G.T., Nurhati, I.S., Pinto, I., Seneviratne, S.I., van den Hurk, B., Vera, C.S., 2020. An update of IPCC climate reference regions for subcontinental analysis of climate model data: definition and aggregated datasets. Earth Syst. Sci. Data 12, 2959–2970. https://doi.org/10.5194/essd-12-2959-2020.

Jones, C.D., Arora, V., Friedlingstein, P., Bopp, L., Brovkin, V., Dunne, J., Graven, H., Hoffman, F., Ilyina, T., John, J.G., Jung, M., Kawamiya, M., Koven, C., Pongratz, J., Raddatz, T., Randerson, J.T., Zaehle, S., 2016. C4MIP – the coupled climate–carbon cycle model intercomparison project: experimental protocol for CMIP6. Geosci. Model Dev. 9, 2853–2880. https://doi.org/10.5194/gmd-9-2853-2016.

Kooperman, G.J., Chen, Y., Hoffman, F.M., Koven, C.D., Lindsay, K., Pritchard, M.S., Swann, A.L.S., Randerson, J.T., 2018. Forest response to rising CO_2 drives zonally asymmetric rainfall change over tropical land. Nat. Clim. Chang. 8, 434–440. https://doi.org/10.1038/s41558-018-0144-7.

Lammertsma, E.I., de Boer, H.J., Dekker, S.C., Dilcher, D.L., Lotter, A.F., Wagner-Cremer, F., 2011. Global CO_2 rise leads to reduced maximum stomatal conductance in Florida vegetation. Proc. Natl. Acad. Sci. 108, 4035–4040. https://doi.org/10.1073/pnas.1100371108.

Mahlstein, I., Daniel, J.S., Solomon, S., 2013. Pace of shifts in climate regions increases with global temperature. Nat. Clim. Chang. 3, 739–743. https://doi.org/10.1038/nclimate1876.

Malone, A.G.O., 2023. Quantifying who will be affected by shifting climate zones. Geographies 3, 477–498. https://doi.org/10.3390/geographies3030025.

McDermid, S., Nocco, M., Lawston-Parker, P., Keune, J., Pokhrel, Y., Jain, M., Jägermeyr, J., Brocca, L., Massari, C., Jones, A.D., Vahmani, P., Thiery, W., Yao, Y., Bell, A., Chen, L., Dorigo, W., Hanasaki, N., Jasechko, S., Lo, M.-H., Mahmood, R., Mishra, V., Mueller, N.D., Niyogi, D., Rabin, S.S., Sloat, L., Wada, Y., Zappa, L., Chen, F., Cook, B.I., Kim, H., Lombardozzi, D., Polcher, J., Ryu, D., Santanello, J., Satoh, Y., Seneviratne, S., Singh, D., Yokohata, T., 2023. Irrigation in the Earth system. Nat. Rev. Earth Environ. https://doi.org/10.1038/s43017-023-00438-5.

Park, S.-W., Kim, J.-S., Kug, J.-S., 2020. The intensification of Arctic warming as a result of CO_2 physiological forcing. Nat. Commun. 11, 2098. https://doi.org/10.1038/s41467-020-15924-3.

Peel, M.C., Finlayson, B.L., McMahon, T.A., 2007. Updated world map of the Köppen-Geiger climate classification. Hydrol. Earth Syst. Sci. 11, 1633–1644. https://doi.org/10.5194/hess-11-1633-2007.

Rohli, R.V., Andrew Joyner, T., Reynolds, S.J., Shaw, C., Vázquez, J.R., 2015a. Globally Extended Köppen–Geiger climate classification and temporal shifts in terrestrial climatic types. Phys. Geogr. 36, 142–157. https://doi.org/10.1080/02723646.2015.1016382.

Rohli, R.V., Joyner, T.A., Reynolds, S.J., Ballinger, T.J., 2015b. Overlap of global Köppen–Geiger climates, biomes, and soil orders. Phys. Geogr. 36, 158–175. https://doi.org/10.1080/02723646.2015.1016384.

Schädel, C., Rogers, B.M., Lawrence, D.M., Koven, C.D., Brovkin, V., Burke, E.J., Genet, H., Huntzinger, D.N., Jafarov, E., McGuire, A.D., Riley, W.J., Natali, S.M., 2024. Earth system models must include permafrost carbon processes. Nat. Clim. Chang. https://doi.org/10.1038/s41558-023-01909-9.

Skalák, P., Farda, A., Zahradníček, P., Trnka, M., Hlásny, T., Štěpánek, P., 2018. Projected shift of Köppen–Geiger zones in the central Europe: a first insight into the implications for ecosystems and the society. Int. J. Climatol. 38, 3595–3606. https://doi.org/10.1002/joc.5520.

Skinner, C.B., Poulsen, C.J., Mankin, J.S., 2018. Amplification of heat extremes by plant CO_2 physiological forcing. Nat. Commun. 9, 1094. https://doi.org/10.1038/s41467-018-03472-w.

Sohoulande, C.D.D., 2023. Vegetation and water resource variability within the Köppen-Geiger global climate classification scheme: a probabilistic interpretation. Theor. Appl. Climatol. https://doi.org/10.1007/s00704-023-04682-z.

Wang, W., Pijl, A., Tarolli, P., 2022. Future climate-zone shifts are threatening steep-slope agriculture. Nat. Food 3, 193–196. https://doi.org/10.1038/s43016-021-00454-y.

Watson, L., Straatsma, M.W., Wanders, N., Verstegen, J.A., de Jong, S.M., Karssenberg, D., 2020. Global ecosystem service values in climate class transitions. Environ. Res. Lett. 15, 024008 https://doi.org/10.1088/1748-9326/ab5aab.

Webb, E.E., Alexander, H.D., Paulson, A.K., Loranty, M.M., DeMarco, J., Talucci, A.C., Spektor, V., Zimov, N., Lichstein, J.W., 2024. Fire-induced carbon loss and tree mortality in Siberian larch forests. Geophys. Res. Lett. 51 https://doi.org/10.1029/2023GL105216.

Wu, B., Lang, X., Jiang, D., 2021. Köppen climate zones in China over the last 21,000 years. J. Geophys. Res. Atmos. 126, 1–19. https://doi.org/10.1029/2020JD034310.

Zhang, M., Gao, Y., 2023. Time of emergence in climate extremes corresponding to Köppen-Geiger classification. Weather Clim. Extrem. 41, 100593 https://doi.org/10.1016/j.wace.2023.100593.

Zhu, Z., Piao, S., Myneni, R.B., Huang, M., Zeng, Z., Canadell, J.G., Ciais, P., Sitch, S., Friedlingstein, P., Arneth, A., Cao, C., Cheng, L., Kato, E., Koven, C., Li, Y., Lian, X., Liu, Y., Liu, R., Mao, J., Pan, Y., Peng, S., Peñuelas, J., Poulter, B., Pugh, T.A.M., Stocker, B.D., Viovy, N., Wang, X., Wang, Y., Xiao, Z., Yang, H., Zaehle, S., Zeng, N., 2016. Greening of the earth and its drivers. Nat. Clim. Chang. 6, 791.